The 9th European Congress on Computational Methods in Applied Sciences and Engineering
ECCOMAS Congress 2024
3–7 June 2024, Lisboa, Portugal

A PHASE-FIELD APPROACH TO MODEL DUCTILE QUASI-STATIC AND FATIGUE FRACTURE IN SHORT FIBER REINFORCED POLYMER COMPOSITES

AAMIR DEAN[1,2], PAVAN KUMAR ASUR[3], ELSADIG MAHDI[4] AND RAIMUND ROLFES[5]

[1] Institute of Structural Analysis
Leibniz Universität Hannover
Appelstr. 9A, 30167 Hannover, Germany
e-mail: a.dean@isd.uni-hannover.de, www.uni-hannover.de

[2] School of Civil Engineering, College of Engineering
Sudan University of Science and Technology
P. O. Box 72, Khartoum, Sudan
e-mail: a.dean@sustech.edu, www.sustech.edu

[3] Institute of Lightweight Design and Structural Biomechanics
Technische Universität Wien
Getreidemarkt 9, 1060 Vienna, Austria
e-mail: pavan.kumar@ilsb.tuwien.ac.at, www.tuwien.at

[4] Department of Mechanical and Industrial Engineering, College of Engineering
Qatar University
P.O. Box 2713, Doha, Qatar
e-mail: elsadigms@qu.edu.qa, www.qu.edu.qa

[5] Institute of Structural Analysis
Leibniz Universität Hannover
Appelstr. 9A, 30167 Hannover, Germany
e-mail: r.rolfes@isd.uni-hannover.de, www.uni-hannover.de

Key words: SFRPs, Fracture, Fatigue, Phase-Field, FEM

Summary. Fracture events pose a significant obstacle to the widespread use of Short Fiber Reinforced Polymers (SFRPs) in diverse engineering applications, especially in lightweight structures. This contribution introduces a phase-field approach to model ductile fracture events in SFRPs under both quasi-static and fatigue loading conditions. Specifically, we employ an invariant-based anisotropic elasto-plastic material model to describe the macroscopic behavior of SFRPs, incorporating pressure-dependent characteristics. Non-associative plastic evolution is introduced herein to capture realistic plastic deformations. This material model is then consistently integrated with the phase-field approach for modeling ductile fracture. To account for fatigue effects, the free-energy function is modified based on thermodynamic considerations, introducing a degradation of the material's fracture toughness. The theoretical formulation and numerical implementation are presented. The modeling approach's performance is assessed through a series of numerical simulations, demonstrating its applicability and robustness.

1 INTRODUCTION

Modern industry is increasingly focused on developing materials and structures that are environmentally friendly, safe, and highly durable, with reduced operational costs. Fiber Reinforced Polymers (FRPs) have emerged as a key innovation, replacing traditional materials in numerous engineering applications due to their high strength-to-weight ratios, fatigue resistance, and lower maintenance needs. Short Fiber Reinforced Polymers (SFRPs), in particular, offer cost-effective solutions for complex structural components. However, the full load-bearing potential of SFRPs remains underutilized [1].

As the use of composite materials continues to grow, there is a pressing need for a deeper understanding of their complex anisotropic, inhomogeneous, and inelastic behavior. Understanding damage and fracture mechanisms in FRPs is critical for optimizing their use in practical applications, where safety and reliability are paramount. FRP structures are subject to various damage and fracture mechanisms during their service life. While these mechanisms can initiate and evolve independently, they often interact synergistically, leading to complex failure patterns. The difficulty in predicting how these mechanisms lead to structural failure necessitates the use of high safety factors in design and extensive certification testing, as highlighted in [2]. Given the high costs and time-intensive nature of experimental investigations into composite materials, there has been a strong push towards the development of advanced numerical modeling and simulation techniques. These tools are essential for fully leveraging the benefits of composites under different loading conditions. The rapid growth in computational power has facilitated the development of sophisticated predictive models capable of simulating a wide range of complex engineering problems. However, traditional Continuum Mechanics (CM) models face limitations in accurately capturing complex fracture behaviors, prompting the development of non-local Continuum Damage Mechanics (CDM) theories and strong discontinuity methods [3, 4, 5]. Despite advancements, these methods still struggle with complex fracture problems, especially in three-dimensional scenarios.

In recent decades, the Phase-Field (PF) method has emerged as a promising alternative for overcoming the limitations of other fracture modeling techniques. Rooted in Griffith's energetic approach to Fracture Mechanics (FM), the PF method regularizes sharp crack discontinuities into a smooth, diffusive field, while preserving the continuity of the displacement field. This makes it particularly well-suited for modeling complex crack patterns [6, 7]. Despite the significant advancements in PF methods, their application has been predominantly focused on brittle materials. However, the inherent flexibility of PF methods allows for the incorporation of phenomenological or physically motivated failure criteria, enabling their application to a broader range of materials, including brittle, quasi-brittle, and ductile materials. This paper aims to extend the PF approach to the prediction of quasi-static and fatigue fracture in SFRPs, providing a robust tool for designing more reliable and cost-effective composite components.

The structure of the paper is as follows: Section 2 outlines the fundamental aspects of the proposed phase-field model. Section 3 presents several numerical examples and discusses the obtained results. Finally, the principal contributions of this study are summarized in Section 4.

2 PHASE-FIELD APPROACH TO FRACTURE

This section concerns the fundamental aspects of the phase-field approach to fracture, then the employment to consider quasi-static and fatigue fracture in SFRPs.

2.1 Variational Formulation

For the application of the PF method within a multi-dimensional framework, let to consider an arbitrary body whose domain is denoted by $\mathcal{B} \in \mathbb{R}^{n_{\text{dim}}}$ ($n_{\text{dim}} = 1, 2, 3$ is the number of spatial dimensions). The delimiting boundary of $\mathcal{B}$ is identified by $\partial\mathcal{B} \in \mathbb{R}^{n_{\text{dim}}-1}$.

The key concept for the phase-field approach to fracture comprises the regularization of a sharp crack topology Γ_c by a diffusive crack within a diffusive crack zone of width l, Figure 1. This approximation is based on the definition of the so-called crack phase-field variable $\mathfrak{d} : \mathcal{B} \times [0, t] \rightarrow [0, 1]$, which is a smooth function within the domain, characterizing for $\mathfrak{d} = 0$ and $\mathfrak{d} = 1$ the intact and the cracked states, respectively. This variable is defined within the body under consideration $\mathcal{B}$ and its evolution is ruled by a suitable temporal expression within the time interval $[0, t]$ along the deformation process. Based on this and recalling mathematical arguments in the spirit of the Γ-convergence concept [8], the fracture energy can be approximated by:

$$\int_{\Gamma_c} \mathcal{G}_c \mathrm{d}\Gamma_c \approx \int_{\mathcal{B}} \mathcal{G}_c \gamma(\mathfrak{d}, \nabla\mathfrak{d}) \mathrm{d}\Omega, \tag{1}$$

where $\mathcal{G}_c$ is the bulk critical energy release rate and $\gamma(\mathfrak{d}, \nabla\mathfrak{d})$ is the so-called crack surface density functional.

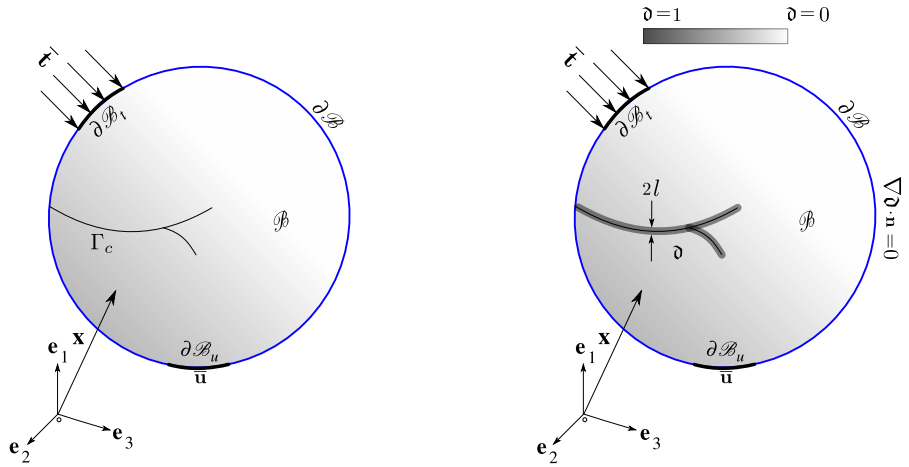

Figure 1: Phase-field method for diffusive crack modelling in solids: (a) sharp crack representation and (b) regularized crack topology

Different authors assumed the quadratic form of the crack surface density functional, which has been successfully applied to isotropic materials [9]:

$$\gamma(\mathfrak{d}, \nabla\mathfrak{d}) = \frac{1}{2l}\mathfrak{d}^2 + \frac{l}{2}\left|\nabla\mathfrak{d}\right|^2. \tag{2}$$

Note, that the expression above is also governed by the length scale parameter l which can be related to the apparent material strength [10]:

$$l = \frac{27}{256}\frac{E\mathcal{G}_c}{\sigma_s^2}, \tag{3}$$

where E denotes the Young modulus and σ_s is the material strength. The *total internal pseudo-energy density* W is postulated as follows:

$$W(\boldsymbol{\varepsilon}, \mathfrak{d}, \nabla\mathfrak{d}) = \Psi(\boldsymbol{\varepsilon}, \mathfrak{d}) + W_{\text{frac}}(\mathfrak{d}, \nabla\mathfrak{d}), \tag{4}$$

where $\Psi(\boldsymbol{\varepsilon}, \mathfrak{d})$ is the bulk free-energy per unit volume and $W_{\text{frac}}(\mathfrak{d}, \nabla\mathfrak{d})$ corresponds to the fracture counterpart. The free-energy is assumed to comply with the simple form:

$$\Psi(\boldsymbol{\varepsilon}, \mathfrak{d}) = g(\mathfrak{d})\Psi^e(\boldsymbol{\varepsilon}), \tag{5}$$

where $\Psi^e(\boldsymbol{\varepsilon})$ is the effective elastic strain energy for uncracked material. The degradation function can be expressed by the simple form $g(\mathfrak{d}) = (1-\mathfrak{d})^2$. In the spirit of Griffith's theory, the fracture term reads:

$$W_{\text{frac}}(\mathfrak{d}, \nabla\mathfrak{d}) = \mathcal{G}_c\ \gamma(\mathfrak{d}, \nabla\mathfrak{d}) = \mathcal{G}_c\ \left[\frac{1}{2l}\mathfrak{d}^2 + \frac{l}{2}\left|\nabla\mathfrak{d}\right|^2\right]. \tag{6}$$

The energy functional that postulates the phase-field method to fracture is given by:

$$\Pi(\mathbf{u}, \mathfrak{d}) = \Pi_{\text{int}}(\mathbf{u}, \mathfrak{d}) + \Pi_{\text{ext}}(\mathbf{u}), \tag{7}$$

where $\Pi_{\text{int}}(\mathbf{u}, \mathfrak{d})$ and $\Pi_{\text{ext}}(\mathbf{u})$ are the internal and external contribution to the energy functional, respectively:

$$\Pi_{\text{int}}(\mathbf{u}, \mathfrak{d}) = \int_{\mathcal{B}} W(\boldsymbol{\varepsilon}, \mathfrak{d}, \nabla\mathfrak{d})\mathrm{d}\Omega = \int_{\mathcal{B}} \Psi(\boldsymbol{\varepsilon}\left(\mathbf{u}\right), \mathfrak{d})\mathrm{d}\Omega + \int_{\mathcal{B}} \mathcal{G}_c\gamma(\mathfrak{d}, \nabla\mathfrak{d})\mathrm{d}\Omega, \tag{8}$$

$$\Pi_{\text{ext}}(\mathbf{u}) = -\int_{\mathcal{B}} \mathbf{f}_v \cdot \mathbf{u}\mathrm{d}\Omega - \int_{\partial\mathcal{B}_t} \bar{\mathbf{t}} \cdot \mathbf{u}\mathrm{d}\partial\Omega, \tag{9}$$

where $\mathbf{f}_v$ and $\bar{\mathbf{t}}$ are the prescribed body actions and applied traction, respectively. The principle of least action to find the stationary path of the system:

$$\delta\Pi(\mathbf{u}, \mathfrak{d}, \delta\mathbf{u}, \delta\mathfrak{d}) = \delta\Pi_{\text{int}}(\mathbf{u}, \mathfrak{d}, \delta\mathbf{u}, \delta\mathfrak{d}) + \delta\Pi_{\text{ext}}(\mathbf{u}, \delta\mathbf{u}) = 0. \tag{10}$$

The strong form of the field equations is then reached:

$$\mathrm{div}\boldsymbol{\sigma} + \mathbf{f}_v = \mathbf{0} \text{ in } \mathcal{B} \text{ and } \boldsymbol{\sigma} \cdot \mathbf{n} = \bar{\mathbf{t}} \text{ on } \partial\mathcal{B}_t, \tag{11}$$

$$2(1-\mathfrak{d})\mathcal{H} = \frac{\mathcal{G}_c}{l}(\mathfrak{d} - l^2\nabla^2\mathfrak{d}) \text{ in } \mathcal{B} \text{ and } \nabla\mathfrak{d} \cdot \mathbf{n} = 0 \text{ on } \partial\mathcal{B}, \tag{12}$$

where $\mathcal{H}$ is the so-called crack driving force. Following the standard Bubnov-Galerkin method, the trial solutions of the two primary fields with:

$$\mathbf{u} \in \mathcal{U}_u := \left\{\mathbf{u} \in H^1(\mathcal{B}) | \nabla\mathbf{u} \in L^2(\mathcal{B});\ \mathbf{u} = \bar{\mathbf{u}} \text{ on } \partial\mathcal{B}_u\right\}, \tag{13}$$

$$\mathfrak{d} \in \mathcal{U}_{\mathfrak{d}} := \left\{\mathfrak{d} \in H^1(\mathcal{B}) | \mathfrak{d}(\mathbf{x}) \in [0,1],\ \dot{\mathfrak{d}} \geq 0,\ \forall\mathbf{x} \in \mathcal{B}\right\}, \tag{14}$$

are extended by the corresponding test functions:

$$\delta\mathbf{u} \in \mathcal{V}_u := \left\{\delta\mathbf{u} \in H^1(\mathcal{B}) | \nabla\delta\mathbf{u} \in L^2(\mathcal{B});\ \delta\mathbf{u} = \mathbf{0} \text{ on } \partial\mathcal{B}_u\right\}, \tag{15}$$

$$\delta\mathfrak{d} \in \mathcal{V}_\mathfrak{d} := \left\{\delta\mathfrak{d} \in H^1(\mathcal{B}) | \delta\mathfrak{d} \geq 0,\ \forall\mathbf{x} \in \mathcal{B}\right\}. \tag{16}$$

The Karush-Kuhn-Tucker (KKT) conditions read:

$$\dot{\mathfrak{d}} \geq 0, \tag{17}$$

$$2(1-\mathfrak{d})\mathcal{H} - \frac{\mathcal{G}_c}{l}(\mathfrak{d} - l^2\nabla^2\mathfrak{d}) \leq 0, \tag{18}$$

$$\left(2(1-\mathfrak{d})\mathcal{H} - \frac{\mathcal{G}_c}{l}(\mathfrak{d} - l^2\nabla^2\mathfrak{d})\right)\dot{\mathfrak{d}} = 0. \tag{19}$$

Exploiting the concept of crack driving force $\mathcal{H}$ but including a phenomenological failure criterion yields:

$$\mathcal{H} = \xi\left[\langle\frac{\max\limits_{\tau\in[0,t]}\Psi^e(\tau)}{\Psi^e_{\text{init}}} - 1\rangle_+\right], \tag{20}$$

where Ψ^e_{init} is the effective elastic energy for crack initiation and ξ is a dimensionless parameter that triggers the activation of fracture.

2.2 Anisotropic and Ductile Fracture

Anisotropic crack density functional is given by [11]:

$$\gamma(\mathfrak{d}, \nabla\mathfrak{d}, \mathbf{A}) = \frac{1}{2l}\mathfrak{d}^2 + \frac{l}{2}\nabla\mathfrak{d}\cdot\overline{\mathbf{A}}\cdot\nabla\mathfrak{d}, \tag{21}$$

where $\overline{\mathbf{A}} = \mathbf{1} + \overline{\alpha}\mathbf{A}$ is a second-order tensor reflecting the material anisotropy, $\mathbf{1}$ denotes the second-order identity, $\overline{\alpha}$ stands for a parameter that weights the material direction $\mathbf{a}$, and the so-called structural tensor defined as $\mathbf{A} = \mathbf{a}\otimes\mathbf{a}$. The pseudo-energy density W for anisotropic elasto-plastic solids:

$$\begin{aligned} W(\boldsymbol{\varepsilon}, \boldsymbol{\varepsilon}^p, \boldsymbol{\varepsilon}^p, \mathfrak{d}, \nabla\mathfrak{d}, \mathbf{A}) = \Psi^e(\boldsymbol{\varepsilon} - \boldsymbol{\varepsilon}^p, \mathfrak{d}, \mathbf{A}) + \Psi^p(\boldsymbol{\varepsilon}^p, \mathfrak{d}, \mathbf{A}) \\ + W_{\text{frac}}(\mathfrak{d}, \nabla\mathfrak{d}, \mathbf{A}), \end{aligned} \tag{22}$$

where $\Psi^e(\boldsymbol{\varepsilon}-\boldsymbol{\varepsilon}^p, \mathfrak{d}, \mathbf{A})$ is the elastic bulk energy, $\Psi^p(\boldsymbol{\varepsilon}^p, \mathfrak{d}, \mathbf{A})$ is the energy contribution associated with the plastic deformation and $W_{\text{frac}}(\mathfrak{d}, \nabla\mathfrak{d}, \mathbf{A})$ corresponds to the fracture counterpart. The elastic contribution is assumed to comply with the simple form:

$$\Psi^e(\boldsymbol{\varepsilon} - \boldsymbol{\varepsilon}^p, \mathfrak{d}, \mathbf{A}) = g(\mathfrak{d})\hat{\Psi}^e(\boldsymbol{\varepsilon}^e, \mathbf{A}), \tag{23}$$

where $\hat{\Psi}^e(\boldsymbol{\varepsilon}^e, \mathbf{A})$ is the effective elastic strain energy for undamaged material.

Similarly, the plastic contribution renders:

$$\Psi^p(\boldsymbol{\varepsilon}^p, \mathfrak{d}, \mathbf{A}) = g(\mathfrak{d})\hat{\Psi}^p(\boldsymbol{\varepsilon}^p, \mathbf{A}). \tag{24}$$

The anisotropic fracture energy contribution then reads:

$$W_{\text{frac}}(\mathfrak{d}, \nabla\mathfrak{d}, \mathbf{A}) = \mathcal{G}_c \; \gamma(\mathfrak{d}, \nabla\mathfrak{d}, \mathbf{A}) = \mathcal{G}_c \; \left[\frac{1}{2l}\mathfrak{d}^2 + \frac{l}{2}\nabla\mathfrak{d} \cdot \overline{\mathbf{A}} \cdot \nabla\mathfrak{d}\right]. \tag{25}$$

The following form of the crack driving force is postulated:

$$\mathcal{H} = \xi^e \left[\langle \frac{\max\limits_{\tau\in[0,t]} \hat{\Psi}^e(\tau)}{\hat{\Psi}^e_{\text{init}}} - 1\rangle_+\right] + \xi^p \left[\langle \frac{\hat{\Psi}^p}{\hat{\Psi}^p_{\text{init}}} - 1\rangle_+\right], \tag{26}$$

where $\hat{\Psi}^e_{\text{init}}$ is the effective elastic energy for crack initiation and ξ^e is a dimensionless parameter that triggers the activation of crack. Similarly, $\hat{\Psi}^p_{\text{init}}$ is the effective plastic energy for crack initiation and ξ^p is a parameter that tracking the activation plastic-induced fracture. The pressure-dependent elasto-plastic model is equipped with a quadratic form of the yield function $\mathcal{F}(\hat{\boldsymbol{\sigma}}, \mathbf{A}, \bar{\varepsilon}^p)$ renders [12]:

$$\mathcal{F}(\hat{\boldsymbol{\sigma}}, \mathbf{A}, \bar{\varepsilon}^p) = \zeta_1 I_1 + \zeta_2 I_2 + \zeta_3 I_3 + \zeta_4 I_3^2 + \zeta_5 I_4 + \zeta_6 I_4^2 - 1 \leq 0, \tag{27}$$

where I_i $(i = 1, 4)$ correspond to the family of the stress invariants representing the integrity basis. $\zeta_i(\bar{\varepsilon}^p)$ $(i = 1, 6)$ stands for the corresponding yield parameters and $\bar{\varepsilon}^p$ is the equivalent plastic strain. The non-associative plastic potential function reads:

$$\mathcal{M}(\hat{\boldsymbol{\sigma}}, \mathbf{A}) = \varsigma_1 I_1 + \varsigma_2 I_2 + \varsigma_3 I_3^2 + \varsigma_4 I_4^2 - 1, \tag{28}$$

where ς_i $(i = 1, 4)$ denotes the plastic potential parameters. Figure 2 depicts an schematic representation of the transversely isotropic yield function in the stress and invariant space.

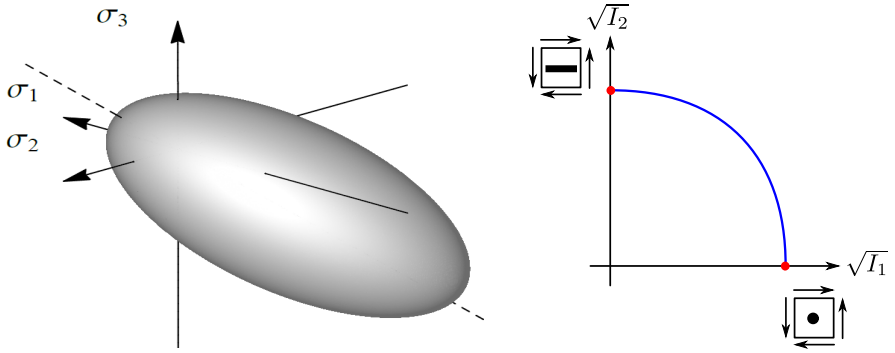

Figure 2: Schematic representation of the transversely isotropic yield function: stress space (left) and (right) invariant space.

2.3 Fatigue Fracture

Keeping the spirit of Griffith's theory, the modified fracture term reads:

$$W_{\text{frac}}(\mathfrak{d}, \nabla\mathfrak{d}, \mathbf{A}, \bar{\kappa}) = \mathcal{Y}(\bar{\kappa})\mathcal{G}_c \; \gamma(\mathfrak{d}, \nabla\mathfrak{d}, \mathbf{A}), \tag{29}$$

where $\bar{\kappa}$ is a local energy accumulation variable and $\mathcal{Y}(\bar{\kappa})$ represents a fatigue degradation function. A symptotic degradation function is defined as [13]:

$$\mathcal{Y}(\bar{\kappa}) = \begin{cases} 1 & \text{if } \bar{\kappa}(t) \leq \kappa_T \\ \left[1 - k\, log \dfrac{\bar{\kappa}(t)}{\kappa_T}\right]^2 & \text{if } \kappa_T \leq \bar{\kappa}(t) \leq \kappa_T 10^{\frac{1}{k}}. \\ 0 & \text{if } \bar{\kappa}(t) \geq \kappa_T 10^{\frac{1}{k}} \end{cases} \tag{30}$$

Here, κ_T and k are material constants that are used to control the fatigue degradation.

3 NUMERICAL EXAMPLES

The resultant nonlinear system of equations is implemented in the finite element software ABAQUS using a two-layer structure corresponding to the displacement field and the phase field. Each layer shares the same nodes but has different stiffness properties and Degrees of Freedom (DOFs). The elements in the first layer have three DOFs, while those in the second layer have one DOF associated with the phase field. Here, PA6GF30 (Polyamide 6 with 30% Glass Fiber) SFRPs sheets are considered, and the constitutive model is calibrated based on the experimental results provided in [14, 15, 16, 12] and the references therein. The elastic material constants are listed in Table 1.

Table 1: Elastic properties

E_{11} (MPa)	E_{22} (MPa)	G_{12} (MPa)	ν_{12} (minor)	ν_{23}
7893	3348	1601	0.175	0.4

Following the procedure presented in [12, 17], the yield function parameters ζ_i $(i = 1, 6)$, which characterize the onset of yielding, are listed in Table 2.

Table 2: Yielding parameters ζ_i at the onset of yielding

ζ_1	ζ_2	ζ_3	ζ_4	ζ_5	ζ_6
0.00262532	0.00179157	−0.0097352	0.00411623	−0.0125167	0.00121853

The plastic potential function parameters ς_i $(i = 2, 4)$ are obtained according to [12, 17] from the plastic Poisson's ratios provided in Table 3.

Table 3: Plastic Poisson's ratios

μ^p_{12}	ν^p_{12} (minor)	ν^p_{23}
1.0	0.167	0.4

Furthermore, the failure criterion coefficients ξ_i $(i = 1, 6)$ that define the onset of failure are listed in Table 4. In addition, the fracture, crack driving force, and fatigue degradation parameters are reported in Table 5.

3.1 Single-Edge Notched Specimen: Quasi-Static Loading

In this study, the failure of a 90° single-edge notched specimen made of PA6GF30 is investigated under pure tension, where the loading direction is perpendicular to the material's internal

Table 4: PA6GF30 (1mm in thickness): failure parameters ξ_i at the onset of failure

ξ_1	ξ_2	ξ_3	ξ_4	ξ_5	ξ_6
0.000232295	0.000158522	−0.00289583	0.000364213	−0.00372321	0.000107818

Table 5: Fracture, crack driving force, and fatigue degradation parameters

$\mathcal{G}^c$ (N/mm)	ξ^e (-)	ξ^p (-)	k (-)	κ_T (-)
3.25	3.5 (assumed)	3.5 (assumed)	0.1	2.0

fiber orientation. Figure 3 illustrates the test specimen, including its finite element (FE) discretization and boundary conditions. The phase-field length scale parameter l is set to 0.215 mm, and the specimen is subjected to displacement-controlled loading. Figure 4 shows the crack phase-field parameter at various loading stages. As anticipated, the crack propagates horizontally at a 90° angle relative to the loading direction, beginning at the notch tip and extending horizontally throughout the simulation. The concurrent evolution of plastic deformations and the cracking process for a representative element is depicted in Figure 5.

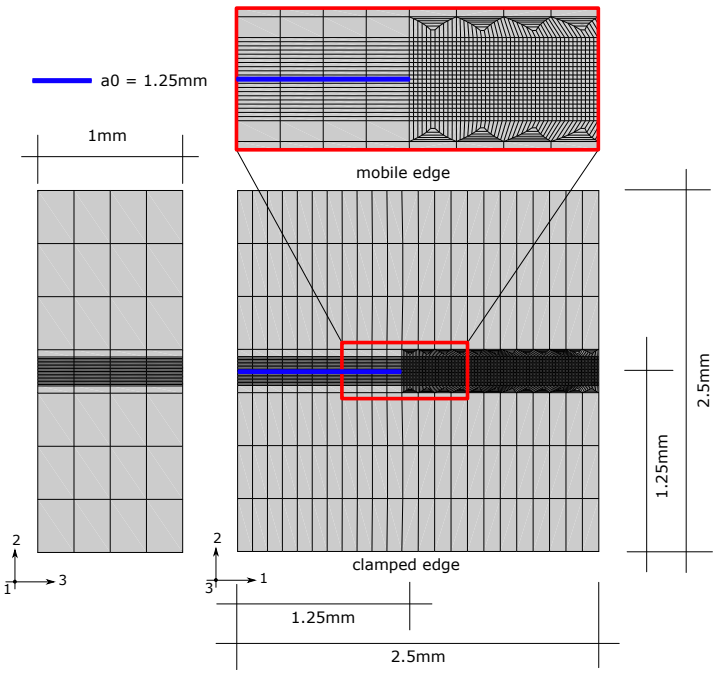

Figure 3: Single-edge notched specimen of PA6GF30: specimen definition, FE discretization, and boundary conditions.

3.2 Dog-Bone Specimen: Cyclic Loading

Here, a dog-bone specimen is utilized to demonstrate the proposed fatigue formulation and its effectiveness in predicting fatigue degradation in SFRPs under cyclic loading. Figure 6 (top) shows the specimen's geometry, finite element discretization, and boundary conditions. The

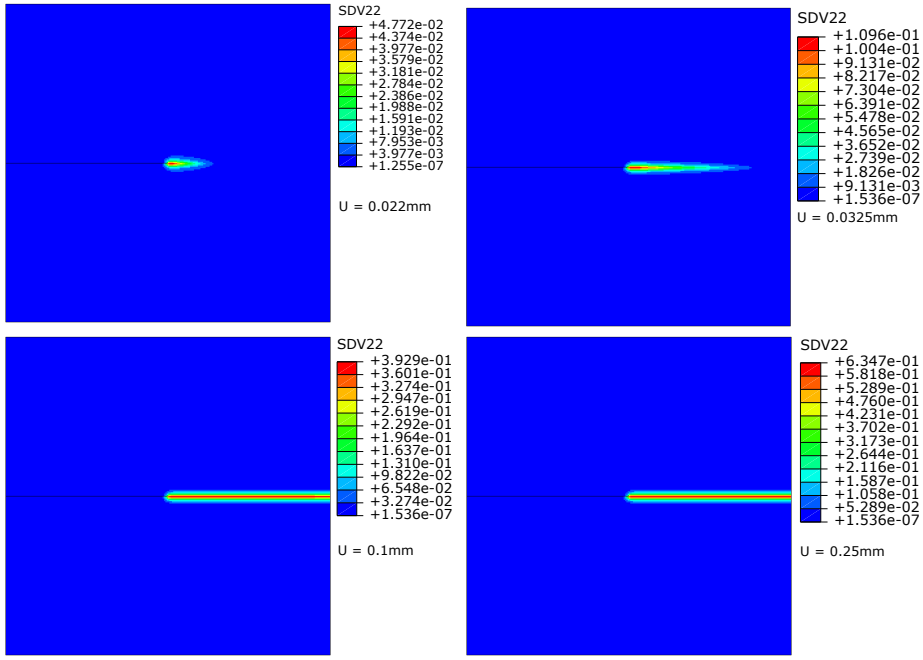

Figure 4: Ductile fracture of the single-edge notched specimen of PA6GF30: phase-field parameter (SDV22) evolution at different loading stages.

phase-field length scale parameter l is set to 0.291 mm. The specimen undergoes cyclic loading controlled by displacement with a stress ratio (R) of 0. Figure 6 (bottom) presents the evolution of various parameters against the number of cycles for a selected element. It includes the applied strain, crack driving force, phase-field parameter, and resultant stresses. As anticipated, the crack driving force progressively accumulates and increases with each loading cycle. Crack initiation and propagation occur only once this force surpasses a critical threshold, leading to a significant degradation in stress. This behavior underscores the capability of the proposed formulation to capture the fatigue response and degradation process in SFRPs under cyclic loading conditions.

3.3 Single-Edge Notched Specimen: Cyclic Loading

Here, the single-edge notched specimen is subjected to cyclic loading under displacement control with a stress ratio R=0. Figure 7 illustrates the evolution of the phase-field parameter at various points along the crack path, highlighting the stages of crack initiation, propagation, and eventual failure at different time instances (i.e., the number of cycles). The figure provides a detailed view of how the crack evolves over time, showcasing the changes in the phase-field parameter as the crack advances. Additionally, the relationship between crack growth and the number of cycles is plotted, demonstrating the material's fatigue behavior. This plot naturally conforms to Paris' law, which validates the effectiveness of the proposed fatigue formulation in predicting crack growth and material degradation under cyclic loading conditions.

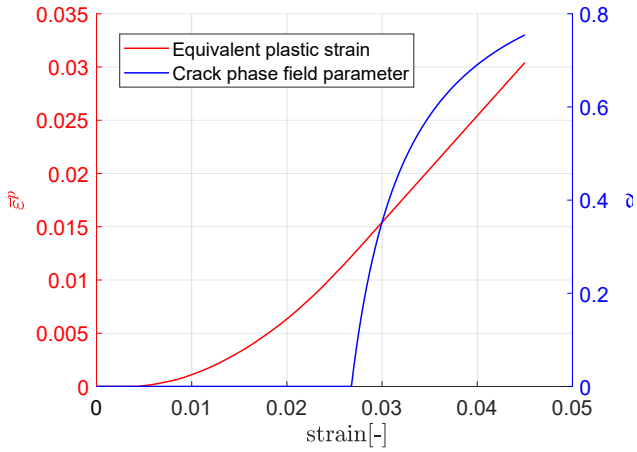

Figure 5: Simultaneous evolution of the plastic deformations and the cracking process.

4 CONCLUSIONS

This study demonstrates that the Phase-Field (PF) method is a powerful tool for modeling fracture behavior in Short Fiber Reinforced Polymers (SFRPs). The PF approach effectively captures both quasi-static and fatigue fracture mechanisms by transforming sharp crack discontinuities into a diffusive field, which facilitates detailed and accurate simulation of complex crack patterns. By incorporating a phenomenological failure criterion that accounts for both elastic and plastic deformations, the model provides a comprehensive framework for predicting fracture behavior in SFRPs. Numerical simulations confirm that the PF method offers significant improvements in both accuracy and computational efficiency compared to traditional methods. This advancement is crucial for designing more reliable and cost-effective SFRPs components, as it allows for better prediction of material performance under various loading conditions. Overall, the PF method represents a valuable contribution to the field of composite material design and fracture mechanics, paving the way for future developments in the modeling and analysis of advanced composite structures.

REFERENCES

[1] M. Zoghi, The International Handbook Of FRP Composites In Civil Engineering, CRC Press, 2013.

[2] Composite Materials Handbook, SAE International, 2017.

[3] G. Maugin, W. Muschik, Thermodynamics with internal variables part II. applications, Journal of Non-Equilibrium Thermodynamics 19 (1994) 250 – 289.

[4] H. Frémond, Non-Smooth Thermomechanics, Springer, 2001.

[5] P. Asur Vijaya Kumar, A. Dean, J. Reinoso, , M. Paggi, Nonlinear thermo-elastic phase-field fracture of thin-walled structures relying on solid shell concepts, Computer Methods in Applied Mechanics and Engineering 396 (2022) 115096.

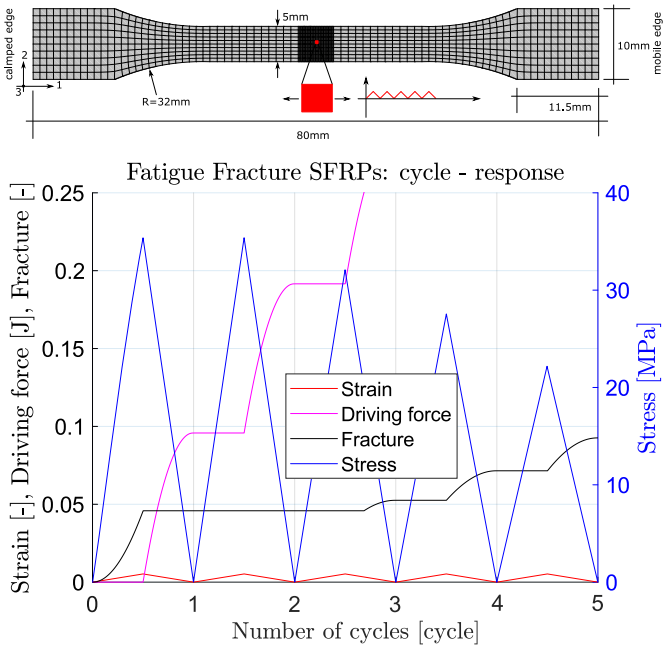

Figure 6: Uniaxial loading fatigue test: (top) dog-bone specimen of PA6GF30 and (bottom) fatigue response.

[6] G. Francfort, J. Marigo, Revisiting brittle fracture as an energy minimization problem, Journal of the Mechanics and Physics of Solids 46 (1998) 1319 – 1342.

[7] B. Bourdin, G. Francfort, J. Marigo, The variational approach to fracture, Journal of Elasticity 91 (2008) 5 – 148.

[8] P. Asur Vijaya Kumar, A. Dean, J. Reinoso, P. Lenarda, M. Paggi, Phase field modeling of fracture in functionally graded materials: γ-convergence and mechanical insight on the effect of grading, Thin-Walled Structures 159 (2021) 107234.

[9] K. Seles, F. Aldakheel, Z. Tonkovic, J. Soric, P. Wriggers, A general phase-field model for fatigue failure in brittle and ductile solids, Computational Mechanics 67 (2021) 1431 – 1452.

[10] E. Tanné, T. Li, B. Bourdin, J. Marigo, C. Maurini, Crack nucleation in variational phase-field models of brittle fracture, Journal of the Mechanics and Physics of Solids 110 (2018) 80 – 99.

[11] A. Dean, P. K. A. V. Kumar, J. Reinoso, C. Gerendt, M. Paggi, E. Mahdi, R. Rolfes, A phase field approach for ductile fracture of short fibre reinforced composites, Composite Structures 251 (2020) 112446.

[12] A. Dean, N. Grbic, R. Rolfes, B. Behrens, Macro-mechanical modeling and experimental validation of anisotropic, pressure- and temperature-dependent behavior of short fiber composites, Composite Structures 211 (2019) 630–643.

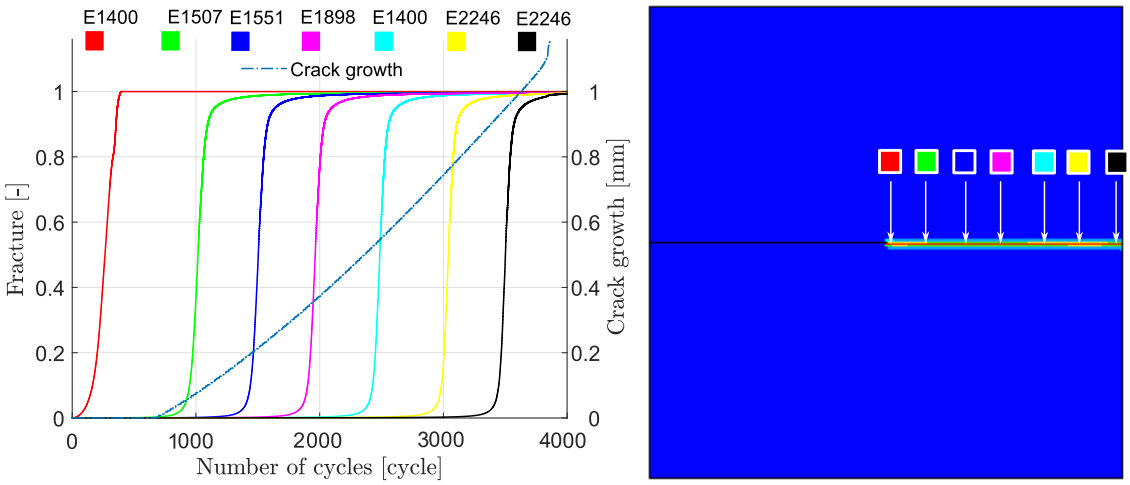

Figure 7: Ductile fatigue fracture of the single-edge notched specimen of PA6GF30: fracture evolution at different elements along the crack path and crack growth.

[13] P. K. Asur Vijaya Kumar, A. Dean, J. Reinoso, H. E. Pettermann, M. Paggi, A phase-field fracture model for fatigue using locking-free solid shell finite elements: Analysis for homogeneous materials and layered composites, Theoretical and Applied Fracture Mechanics 127 (2023) 104029.

[14] A. Dean, S. Sahraee, J. Reinoso, R. Rolfes, Finite deformation model for short fibre reinforced composites: Application to hybrid metal-composite clinching joints, Composite Structures 150 (2016) 162 – 171.

[15] A. Dean, J. Reinoso, S. Sahraee, R. Rolfes, An invariant-based anisotropic material model for short fiber-reinforced thermoplastics: Coupled thermo-plastic formulation, Composites Part A: Applied Science and Manufacturing 90 (2016) 186 – 199.

[16] A. Dean, S. Sahraee, J. Reinoso, R. Rolfes, A new invariant-based thermo-plastic model for finite deformation analysis of short fibre reinforced composites: Development and numerical aspects, Composites Part B: Engineering 125 (2017) 241 – 258.

[17] A. Dean, J. Reinoso, N. K. Jha, E. Mahdi, R. Rolfes, A phase field approach for ductile fracture of short fibre reinforced composites, Theoretical and Applied Fracture Mechanics 106 (2020) 102495.